Eur. Phys. J. Special Topics **216**, 181–190 (2013)

DOI: 10.1140/epjst/e2013-01741-3

THE EUROPEAN PHYSICAL JOURNAL SPECIAL TOPICS

Regular Article

Polymer-attractive spherical cage system

Handan Arkın[1,2,a] and Wolfhard Janke[1,b]

[1] Institut für Theoretische Physik, Universität Leipzig, Postfach 100 920, 04009 Leipzig, Germany
[2] Department of Physics Engineering, Faculty of Engineering, Ankara University, Tandogan, 06100 Ankara, Turkey

Received 30 November 2012 / Received in final form 6 December 2012
Published online 31 January 2013

Abstract. We analyze the structural behavior of a single polymer chain inside an attractive sphere. Our model is composed of a coarse-grained polymer governed by Lennard-Jones interactions of the monomers and an attractive sphere potential which follows by integrating the monomer-monomer interaction over the (inner) surface of the sphere. By means of extensive multicanonical Monte Carlo simulations it is shown that the system exhibits a rich phase diagram in the adsorption strength-temperature ($\epsilon - T$) plane ranging from highly ordered and compact to extended and random coil structures and from desorbed to partially or even completely adsorbed conformations. These findings are identified with different energetic and structural observables. The resulting phase diagram in the $\epsilon - T$ plane is compared with that for a polymer adsorbing to a plane, attractive substrate obtained previously by Möddel, Bachmann, and one of the authors.

1 Introduction

The structure formation of polymers and proteins in different environments is a fascinating field in interdisciplinary research and nanotechnological applications including, e.g., the fabrication of biosensors [1] or peptide adhesion [2] to metals [3,4] and semiconductors [5–7]. Within this context, it seems quite important to gain a deeper knowledge of the problem by starting from the very origins using simplified polymer models. Despite numerous detailed numerical studies in the past, due to the complexity introduced for instance by the huge number of sequence possibilities for proteins and different kinds of environments in general, many problems are still not well understood. One of the reasons is that the understanding of how the conformational space is affected by the geometric constraint of differently shaped cages depends on several external parameters such as the cage shape and size, surface attraction strength and temperature, whose effects are difficult to disentangle.

Our focus here is on a systematic comparison of a "*polymer–attractive sphere*" cage system [8,9] with a similar model describing polymers interacting with an attractive

[a] e-mail: Handan.Arkin@itp.uni-leipzig.de
[b] e-mail: Wolfhard.Janke@itp.uni-leipzig.de

flat surface [10–12]. Both studies rely on extensive Monte Carlo (MC) computer simulations of minimalistic coarse-grained polymer models which make it possible to elucidate generic features. For instance, it is interesting to understand the mechanism by which proteins and polymers cluster or aggregate on surfaces of different shapes. This provides an insight into the growth behavior of polymer layers and thus may enable the researchers to engineer bioactive shapes having specific properties. Therefore, the theoretical treatment of the adsorption of macromolecules within the framework of minimalistic coarse-grained polymer models in statistical mechanics has been a longstanding problem [13,14] that still attracts a lot of interest [15–22].

2 Model

2.1 Bead-stick polymer model

The polymer chain is described by a coarse-grained off-lattice model for homopolymers which has been adopted from similar studies of heteropolymers [23] within the framework of the hydrophobic-polar model [24–27]. Adjacent monomers are connected by rigid covalent bonds whose length is set to unity. The monomers interact through a 12–6 Lennard-Jones (LJ) potential accounting for short-range excluded volume repulsion and van der Waals interaction. An additional interaction accounts for a (in our case very weak) bending energy of any pair of successive bonds. The position vector of the ith monomer, $i = 1, \ldots, N$, is denoted by $\mathbf{r}_i$, and the distance between monomers is $r_{ij} = |\mathbf{r}_i - \mathbf{r}_j|$. A polymer with N monomers has $N-1$ bonds and $N-2$ bending angles ϑ_i defined through $\cos\vartheta_i = (\mathbf{r}_{i+1} - \mathbf{r}_i) \cdot (\mathbf{r}_{i+2} - \mathbf{r}_{i+1})$. The energy function for the polymer is thus given by

$$E_p = 4 \sum_{i=1}^{N-2} \sum_{j=i+2}^{N} \left(r_{ij}^{-12} - r_{ij}^{-6} \right) + \frac{1}{4} \sum_{i=1}^{N-2} \left(1 - \cos\vartheta_i \right). \tag{1}$$

2.2 Confining attractive sphere potential

In this work we assume that the polymer chain is confined inside an attractive sphere of radius R_c which is a measure of the cage size. The interaction of the polymer chain monomers and the attractive sphere is of van der Waals type, modeled by the usual 12–6 LJ expression

$$V_{\mathrm{LJ}}(r) = 4\epsilon_c \left[\left(\frac{\sigma}{r} \right)^{12} - \epsilon \left(\frac{\sigma}{r} \right)^{6} \right], \tag{2}$$

where σ and ϵ determine the location of the potential minimum, $r^{\min} = (2/\epsilon)^{1/6}\sigma$, and ϵ_c and ϵ set the scale of the minimum depth, $V_{\mathrm{LJ}}^{\min} = V_{\mathrm{LJ}}(r_{\min}) = -\epsilon_c\epsilon^2$. Here, $r = |\mathbf{r}|$ denotes the distance of the ith monomer to the surface of the sphere, where $\mathbf{r} = R_c\mathbf{e}_r - \mathbf{r}_i$ with $\mathbf{e}_r$ being a unit vector in radial direction. Assuming a homogeneous surface density ρ $\left(\rho\sigma^2 \equiv 1\right)$, we integrate this potential over the entire inner surface of the sphere:

$$V_{\mathrm{s}}(r_i) = \rho \int_S dS\, V_{\mathrm{LJ}}(r). \tag{3}$$

By choosing $\mathbf{r}_i$ as z-direction and using spherical coordinates, we have $r^2 = R_c^2 - 2R_c r_i \cos\theta + r_i^2$ (see Fig. 1), such that

$$V_{\mathrm{s}}(r_i) = 4\epsilon_c\rho R_c^2 \int_0^{2\pi} d\phi \int_{-1}^{1} d\cos\theta \left[\left(\frac{\sigma}{r} \right)^{12} - \epsilon \left(\frac{\sigma}{r} \right)^{6} \right]. \tag{4}$$

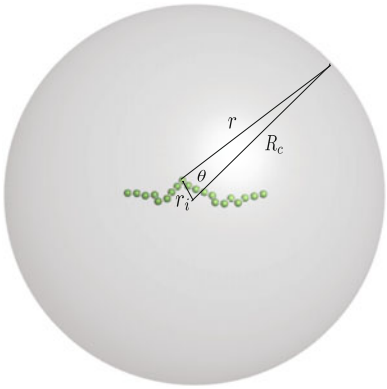

Fig. 1. The graphical representation of the system of a polymer chain inside an attractive sphere. For the sphere radius, we choose $R_c = 20$ to let the polymer with $N = 20$ monomers circulate freely inside the sphere.

The ϕ integral is trivial and the integration over $\cos\theta$ is elementary. Since $r^2 = R_c^2 + 2R_c r_i + r_i^2 = (R_c + r_i)^2$ at the lower limit $\cos\theta = -1$ and $r^2 = R_c^2 - 2R_c r_i + r_i^2 = (R_c - r_i)^2$ at the upper limit $\cos\theta = +1$, one readily obtains

$$V_{\rm s}(r_i) = 4\pi\epsilon_c \frac{R_c}{r_i}\left\{\frac{1}{5}\left[\left(\frac{\sigma}{R_c - r_i}\right)^{10} - \left(\frac{\sigma}{R_c + r_i}\right)^{10}\right] - \frac{\epsilon}{2}\left[\left(\frac{\sigma}{R_c - r_i}\right)^{4} - \left(\frac{\sigma}{R_c + r_i}\right)^{4}\right]\right\}. \tag{5}$$

The parameter ϵ in the second term of Eq. (5) defines the attraction strength of the sphere inner wall and weighs the relative importance of intrinsic monomer-monomer and monomer-sphere wall interactions.

For r_i close to the wall, $r_i \approx R_c$, we can neglect the terms $(\sigma/2R_c)^{10}$ and $\epsilon(\sigma/2R_c)^4$ and approximate

$$V_{\rm s}(r_i) \approx 4\pi\epsilon_c \frac{R_c}{r_i}\left[\frac{1}{5}\left(\frac{\sigma}{R_c - r_i}\right)^{10} - \frac{\epsilon}{2}\left(\frac{\sigma}{R_c - r_i}\right)^{4}\right] \tag{6}$$

$$\approx 4\pi\epsilon_c \left[\frac{1}{5}\left(\frac{\sigma}{R_c - r_i}\right)^{10} - \frac{\epsilon}{2}\left(\frac{\sigma}{R_c - r_i}\right)^{4}\right], \tag{7}$$

which is a standard $10-4$ LJ potential with

$$V_{\rm s}^{\rm min} = -4\pi\epsilon_c \frac{3}{10}\epsilon^{5/3} \qquad \text{at} \qquad r_i^{\rm min} = R_c - \sigma\left(\frac{1}{\epsilon}\right)^{1/6}. \tag{8}$$

The minimum value $V_{\rm s}^{\rm min}$ may be further improved by reinserting $R_c/r_i \approx R_c/r_i^{\rm min} = R_c/(R_c - \sigma\epsilon^{-1/6})$ [recall Eq. (6)], yielding our final approximation

$$V_{\rm s}^{\rm min} \approx -4\pi\epsilon_c \frac{3}{10}\epsilon^{5/3}\frac{R_c}{R_c - \sigma\epsilon^{-1/6}}, \tag{9}$$

which turns out to be extremely accurate over the entire relevant ϵ regime.

In what follows, the parameters σ and ϵ_c are set to unity. The functional dependence of the exact potential $V_{\rm s}$ in Eq. (5) is shown in Fig. 2(a) for $R_c = 20$ and for

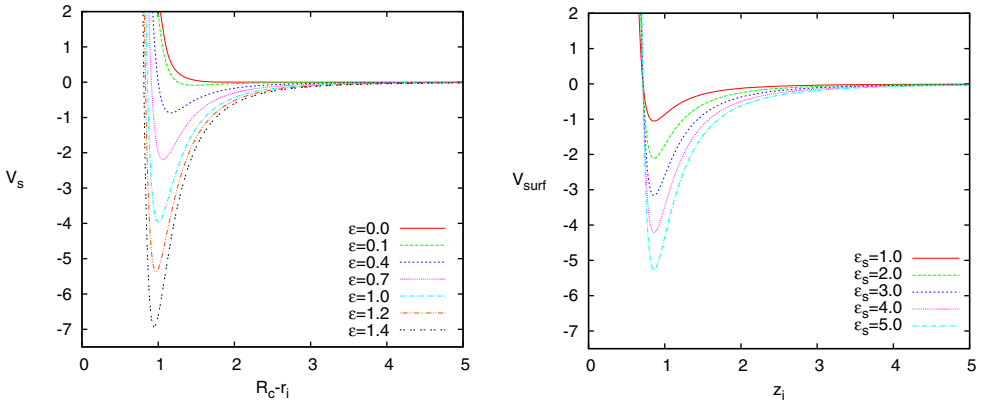

Fig. 2. (a) The attractive sphere potential (5) plotted for $R_c = 20$ and for various values of ϵ. With increasing ϵ, the minimum location varies from $R_c - r_i \approx 1.47$ for $\epsilon = 0.1$ to $R_c - r_i \approx 0.95$ for $\epsilon = 1.4$. (b) The flat surface potential (10) plotted for various values of ϵ_s. Here, the minimum is attained at $z_i \approx 0.8584$ for all ϵ_s.

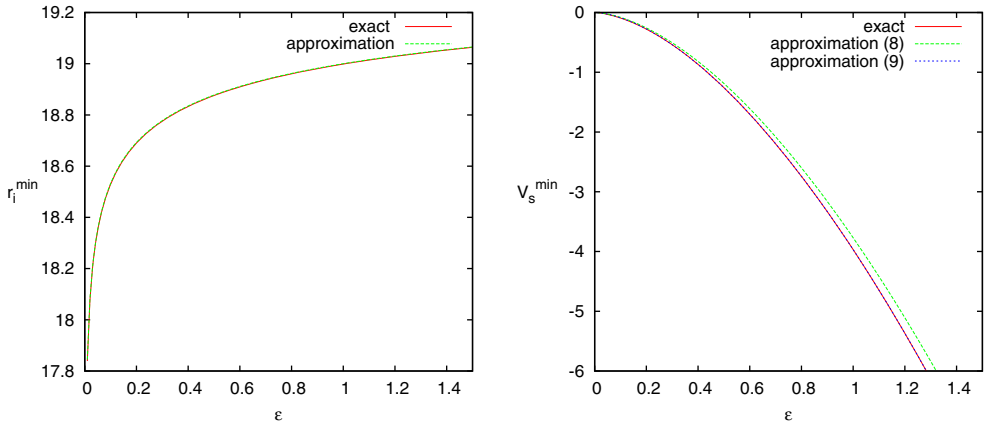

Fig. 3. (a) The position of the minimum and (b) its depth of the attractive sphere potential (5) as a function of ϵ in comparison with the approximations (8) and (9).

selected ϵ values. The minimum varies from $r_i \approx 18.53$ for $\epsilon = 0.1$ to $r_i \approx 19.05$ for $\epsilon = 1.4$. For $\epsilon = 0.0$, the second term vanishes and the sphere potential is purely repulsive. For very small attraction strengths, the functional form of the potential is very shallow meaning that the potential has weak attraction. An increase of ϵ also increases the depth of the potential which then describes a strong attraction. The numerically determined minimum position ($r_i^{\min}$) and the minimum potential value ($V_{\rm s}^{\min}$) of $V_{\rm s}(r_i)$ in Eq. (5) as a function of ϵ are compared in Figs. 3(a) and (b) with the approximations (8) and (9), respectively. On the scale of the graph, the exact curve for $r_i^{\min}$ and the approximation (8) fall on top of each other (agreement better than 0.02%). Also for $V_{\rm s}^{\min}$, the leading-order approximation (8) is already quite good (at a 7% level) and the improved approximation (9) is practically indistinguishable from the exact result (better than 0.01%). This observation renders the discussion of the seemingly complicated surface potential (5) very simple and lets us easily deal with it.

2.3 Attractive flat surface potential

In this study, we compare our results for the sphere potential with recent investigations of an attractive flat surface potential [10–12] which is obtained by integrating over a smooth half-space, where every space element interacts with a single monomer by the usual 12–6 LJ expression. One obtains the potential [28,29]:

$$V_{\text{surf}} = \epsilon_s \left[\frac{2}{15} \left(\frac{1}{z_i} \right)^9 - \left(\frac{1}{z_i} \right)^3 \right], \tag{10}$$

where z_i is the distance of the ith monomer from the flat surface. Minimizing V_{surf} gives

$$V_{\text{surf}}^{\min} = -\frac{2}{3}\sqrt{\frac{5}{2}}\epsilon_s \approx -1.054\epsilon_s \qquad \text{at} \qquad z_i^{\min} = \left(\frac{2}{5} \right)^{1/6} \approx 0.8584. \tag{11}$$

The parameter ϵ_s defines the surface attraction strength, as in our study, and it weighs the energy scales of intrinsic monomer-monomer and monomer-surface attraction. Figure 2(b) shows the functional dependence of the flat surface potential (10) for the selected ϵ_s values.

3 Simulation setup

3.1 Multicanonical method

In order to obtain statistical results of sufficient accuracy, we applied the multicanonical Monte Carlo algorithm [30–33] (for reviews, see Refs. [34,35]), where the energy distribution is flattened artificially allowing, in principle, for a random walk of successive states in energy space. This flattening is controllable and therefore reproducible. To this end, the Boltzmann probability is multiplied by a weight factor $W(E)$, which in our case is a function of the energy. Then, the multicanonical probability for a state $\{\mathbf{x}\}$ with energy $E(\{\mathbf{x}\})$ reads $p_M(E) = \exp(-E/k_BT)W(E)$. In order to obtain a multicanonical or "flat" distribution, the initially unknown weight factor $W(E)$ should be determined iteratively: In the beginning, the weights $W^{(0)}(E)$ are set to unity for all energies letting the first run be a usual Metropolis simulation which yields an estimate $H^{(0)}(E)$ for the canonical distribution. This histogram is used to determine the next guess for the weights, the simplest update being to calculate $W^{(1)}(E) = W^{(0)}(E)/H^{(0)}(E)$. Then, the next run is performed with probabilities $p_M^{(1)}(E) = \exp(-E/k_BT)W^{(1)}(E)$ of states with energy E, yielding $H^{(1)}(E)$ and $W^{(2)}(E) = W^{(1)}(E)/H^{(1)}(E)$, and so on. The iterative procedure is continued until the weights are appropriate in a way that the multicanonical histogram $H(E)$ is "flat". Having determined the accurate weights $W(E)$, they are kept fixed and following some thermalization sweeps, a long production run is performed, where statistical quantities O are obtained multicanonically, $\langle O \rangle_M = \sum_{\{\mathbf{x}\}} p_M(E(\{\mathbf{x}\}))O(\{\mathbf{x}\})/Z_M$ with the multicanonical partition function $Z_M = \sum_{\{\mathbf{x}\}} p_M(E(\{\mathbf{x}\}))$. The canonical statistics is obtained by reweighting the multicanonical to the canonical distribution, i.e., mean values are calculated as $\langle O \rangle = \langle OW^{-1} \rangle_M / \langle W^{-1} \rangle_M$.

3.2 Observables

To obtain as much information as possible on the canonical equilibrium behavior, we calculate energetic (specific heat) and suitable structural quantities O such as the

radius of gyration. Next to the canonical expectation values $\langle O \rangle$, we also determine the fluctuations about these averages, as represented by the temperature derivative $(\langle OE \rangle - \langle O \rangle \langle E \rangle) / T^2$. We use generic units, in which $k_B = 1$. In order to identify the adsorption behavior, we primarily consider the mean number of monomers docked to the surface. The sphere potential is a continuous potential, and in order to distinguish the monomers docked to the sphere inner wall from those not being docked, it is reasonable to introduce a cutoff. We define a monomer i as being "docked" if $R_c - r_i < r_c \equiv 1.2$. The corresponding measured quantity is the average number $\langle N_s \rangle$ of monomers docked to the inner wall.

3.3 Computational details

In our simulations, the polymer chain length is $N = 20$ and we set R_c large enough to enclose the polymer inside the sphere. We also have done simulations with different sizes of the sphere ranging from $R_c = 10, 20, 30$. However, to allow the chain to circulate freely inside the sphere as well as to reduce the effect on the observables, we eventually set it to 20. Different walls are modeled by varying ϵ between 0.1 and 1.4. The total energy of the system is composed of the pure polymer chain energy and the polymer chain attractive sphere interaction energy. A starting configuration of the simulation is sketched in Fig. 1. The initial configuration of the polymer chain is randomly generated where the ends have no contact with the sphere attractive wall.

In order to determine the multicanonical weights we performed 200 iterations with at least 10^5 sweeps each. In the production period, 1×10^8 sweeps were generated to get reasonable statistics for estimating the thermodynamic quantities. Statistical errors are estimated using the standard Jackknife technique [36,37].

4 Results and discussion

4.1 Spherical cage system

The phase structure derived from the specific heat and structural observables is summarized in the pseudophase diagram in the $\epsilon - T$ plane of Fig. 4. The boundaries in the diagram separate the different structural pseudophases labeled by a letter code adopted from Refs. [10,22]. For low attraction strength, the polymer behaves similarly to a free polymer where, below the freezing transition, compact conformations (Desorbed Compact DC) are identified and above globular (Desorbed Globular DG) ones. At higher temperatures, a second transition signals the globular to Desorbed Expanded (DE) transition or, in other words, a random-coil transition. An increase of the attraction strength leads to an increase of the temperature of the adsorption transition. This transition separates desorbed (D) and adsorbed (A) conformations. In the adsorbed region below the collapse transition, there is an adsorbed globular (AG) phase where the conformations look like a drop on the surface. At even higher temperature and ϵ, a partially adsorbed extended phase (AE2) is observed. Except adsorption, collapse and freezing transitions, the most pronounced transition detected by us is the layering transition which comes into play at $\epsilon \approx 1.0$. This transition separates the conformational spaces of planar conformations which are single-layer and totally adsorbed conformations to the sphere inner wall (AC1, AE1) from two-layer (AC2) or three-layer (AC3) and adsorbed spherically compact (AC4) conformations which are seen at ϵ values smaller than $\epsilon \approx 1.0$. The latter structures occur when the attraction strength is not yet strong enough to induce one-layer compact structures but sufficiently high to favour polymer-sphere wall contacts. At a higher temperature,

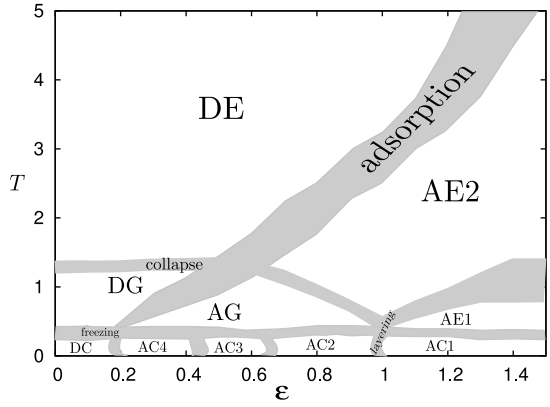

Fig. 4. The pseudophase diagram of the polymer-attractive sphere system as obtained in extensive multicanonical simulations, parametrized by attraction strength ϵ and temperature T. The boundaries separate individual conformational phases. The bandwidth, which reflects the transition regions, shows the variation of the peaks of temperature derivatives of different structural observables which have been analyzed simultaneously. The phases labeled with an "A/D" are adsorbed/desorbed (for details see the text).

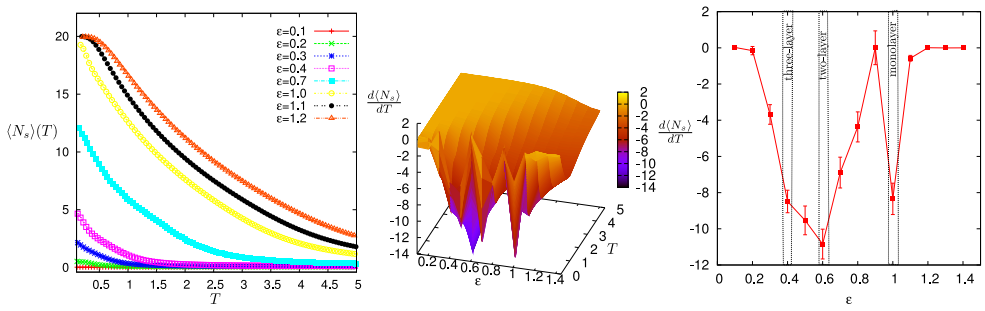

Fig. 5. (a) The average number of adsorbed monomers $\langle N_s \rangle$ at the inner wall of the sphere as a function of temperature T for selected values of ϵ. The starting point of adsorption is around $\epsilon \approx 0.2$. (b) Three-dimensional plot of $d\langle N_s \rangle / dT$ plotted against ϵ and T. (c) The temperature derivative of $\langle N_s \rangle$ at $T = 0.2$ as a function of ϵ.

two different pictures can be distinguished depending on the competition of chain energy and attraction energy. For low ϵ values, the polymer first desorbs (from AG to DG) and then expands at even a higher temperature (from DG to DE). For larger ϵ values, the polymer first expands because it is still adsorbed (from AG to AE2) and then, at higher temperature, desorbs (from AE2 to DE). The AE1 phase occurs for even higher ϵ values.

Since the adsorption transition typically affects only the segments of the polymer, the best way to discuss the adsorption transition is to calculate the average number of monomers docked to the inner wall of the sphere. As can be seen in Fig. 5(a), for large temperatures and small values of ϵ, the polymer can move freely inside the sphere and the effect of the attractive sphere cannot be seen. Thus, the average number of monomer contacts for $\epsilon = 0.1$ is like a straight line at $\langle N_s \rangle = 0$. On the other hand, for high ϵ values and low temperatures, the polymer tends to make surface contacts so that the average number of monomer contacts increases. The first signal of this behavior starts at $\epsilon \approx 0.2$ which can be considered as the adsorption transition. Above

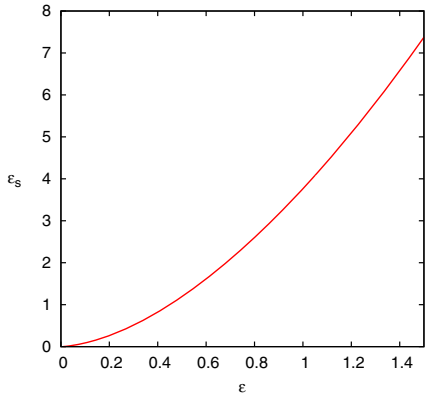

Fig. 6. The attraction strength ϵ_s of the flat substrate as a function of the attraction strength ϵ of the sphere in our parametrization derived in Eq. (12).

$\epsilon = 1.0$, all the monomers are adsorbed to the inner wall of the sphere so that $\langle N_s \rangle$ equals the chain length $N = 20$. As a result, at $\epsilon \approx 1.0$, which is also determined from other structural observables as a more pronounced layering transition, the single-layer structures come into play. The single-layer transition is a topological transition where polymer conformations completely adsorb at the inner wall of the sphere. Also, the fluctuations of the average number of monomer contacts give clear indications of the adsorption transition as well as the layering transition (Fig. 5(b)). In the $\epsilon - T$ plane, the fluctuations of $\langle N_s \rangle$ exhibit three clear deviations which occur at $\epsilon \approx 0.4, 0.6, 1.0$ corresponding to the AC3, AC2, AC1 (layering transition) structures. Along the temperature axis, the inflection points give the adsorption transition temperatures which depend on the ϵ value. A further important result is illustrated in Fig. 5(c), where we plot the temperature derivative of the average number of monomers docked to the inner surface of the sphere, $d\langle N_s \rangle / dT$, at temperature $T = 0.2$ as a function of the attraction strength of the sphere. We observe two peaks and one shoulder corresponding to the three-layer ($\epsilon \approx 0.4$), two-layer ($\epsilon \approx 0.6$) and monolayer ($\epsilon \approx 1.0$) transitions, respectively. Due to a large number of degrees of freedom for the off-lattice polymer, higher-order layering transitions cannot be identified in our analyses.

4.2 Comparison with flat surface system

One goal of the present work is to compare our results discussed in the last subsection with those obtained from a similar model for a polymer interacting with a flat, unstructured substrate via the potential given in Eq. (10). In order to do so, we relate our attraction strength parameter ϵ with the attraction strength of the flat surface ϵ_s. By comparing $V^{\min}$ in the approximation (9) with (11), one finds

$$\epsilon_s = \frac{1}{1.054} 4\pi \frac{3}{10} \epsilon^{5/3} \frac{R_c}{R_c - \epsilon^{-1/6}}. \tag{12}$$

In Fig. 6, the attraction strength of the flat substrate ϵ_s is plotted as a function of our attraction strength ϵ. From this plot we obtained the ϵ_s values for various transitions and compared with the values obtained from simulations in Ref. [10]. Table 1 summarizes the attraction strength values for all low-temperature transitions for the two potentials.

Table 1. Attraction strength values for all low-temperature transitions for the two potentials and chain length $N = 20$.

Transition	V_s	V_{surf} (Eq. (12))	V_{surf} (Ref. [10])
adsorption transition	$\epsilon \approx 0.2$	$\epsilon_s \approx 0.26$	$\epsilon_s \approx 0.2$
transition AC4 $\leftrightarrow$ AC3	$\epsilon \approx 0.4$	$\epsilon_s \approx 0.82$	–
transition AC3 $\leftrightarrow$ AC2	$\epsilon \approx 0.6$	$\epsilon_s \approx 1.61$	$\epsilon_s \approx 1.7$
layering transition AC2 $\leftrightarrow$ AC1	$\epsilon \approx 1.0$	$\epsilon_s \approx 3.76$	$\epsilon_s \approx 3.4$

Although the potentials have some functional differences in the minimum positions and minimum values, we observe quite a good agreement for the location of the low-temperature transition points. Moreover, the adsorption line has certain similarities in both models. There are, however, some differences in the slope, which depends on the system geometry and energy scales and on the extrapolation of the transition line. For chain length $N = 20$, in both models we observe an offset of the adsorption transition line at about $\epsilon = 0.2$ (ϵ_s in the flat case). For longer chains (40mer) [12], this offset seems to shift to smaller ϵ_s values such that the adsorption line may approach the origin for large N.

Semispherical conformations at low T and the transition from two-layer to monolayer conformations, the layering transition, are observed in both models. The layering transition is a very sharp transition in both cases. Also, the shape of the conformations in this transition regime from topologically 3D adsorbed to 2D adsorbed looks very similar. Moreover, the ϵ values of this transition point are in good agreement, as said before, which is found by our mapping (12). On the contrary we also observe the distinction in this region (low T) between the pseudophases AC4 and AC3, whereas in the flat substrate model, these two phases merge for chain length $N = 20$. Similarly, in both models, there exists the AG pseudophase of adsorbed globules.

To conclude, the high-temperature pseudophases DE, DG, AG, and AE, except for some deviations in the slope of the adsorption transition line, nicely correspond to each other in the two models. Differences only occur in those regions in the pseudophase diagram where the compact conformations are dominant and, as expected, will merge in the thermodynamic limit. As a result, for the pseudophases that are assumed to be relevant in the thermodymamic limit, we found a good coincidence.

5 Conclusion

In this paper, the structural behavior of polymers within the framework of a minimalistic coarse-grained homopolymer model inside an attractive sphere is presented. As the attractive sphere potential, a Lennard-Jones type potential between the effective monomers and the sphere wall is assumed and integrated over the whole inner wall of the sphere. All the results obtained from different observables of the polymer-attractive sphere system depending on the attraction strength and temperature are summarized in the pseudophase diagram which gives a good overview of the system under consideration. We compared our results discussed here with those determined from a similar model for a polymer interacting with a flat attractive substrate. Certain similarities between the two studies are found and discussed.

We wish to thank Martin Marenz, Monika Möddel, and Johannes Zierenberg for useful discussions. H.A. acknowledges support by the Alexander von Humboldt Foundation under the Experienced Researcher Fellowship Programme. W.J. thanks the German Research Foundation (DFG) for support under Grant Nos. JA483/24-3 and SFB/TRR 102 project B04. The

computer time for the Monte Carlo simulations was provided by NIC, Forschungszentrum Jülich under Grant No. hlz17 which we gratefully acknowledge.

References

1. R.F. Service, Science **270**, 230 (1995)
2. S. Walheim, E. Schaffer, J. Mlynek, U. Steiner, Science **283**, 520 (1999)
3. S. Brown, Nat. Biotechn. **15**, 269 (1997)
4. R. Braun, M. Sarikaya, K. Schulten, J. Biomater. Sci. Polymer Edn. **13**, 747 (2002)
5. S.R. Whaley, D.S. English, E.L. Hu, P.F. Barbara, A.M. Belcher, Nature **405**, 665 (2000)
6. K. Goede, P. Busch, M. Grundmann, Nano Lett. **4**, 2115 (2004)
7. M. Bachmann, K. Goede, A.G. Beck-Sickinger, M. Grundmann, A. Irbäck, W. Janke, Angew. Chem. Int. Ed. **49**, 9530 (2010)
8. H. Arkın, W. Janke, Phys. Rev. E **85**, 051802 (2012)
9. H. Arkın, W. Janke, J. Phys. Chem. B **116**, 10379 (2012)
10. M. Möddel, M. Bachmann, W. Janke, J. Phys. Chem. B **113**, 3314 (2009)
11. M. Möddel, W. Janke, M. Bachmann, Phys. Chem. Chem. Phys. **12**, 11548 (2010)
12. M. Möddel, W. Janke, M. Bachmann, Macromolecules **44**, 9013 (2011)
13. E. Eisenriegler, *Polymers near Surfaces* (World Scientific, Singapore, 1993)
14. G.J. Fleer, M.A. Cohen Stuart, J.M.H.M. Scheutjens, T. Cosgrove, B. Vincent, *Polymers at Interfaces* (Chapman and Hall, London, 1993)
15. H.W. Diehl, M. Shpot, Nucl. Phys. B **528**, 595 (1998)
16. A. Sikorski, Macromol. Theory Simul. **11**, 359 (2002)
17. M. Bachmann, W. Janke, Phys. Rev. Lett. **95**, 058102 (2005)
18. M. Bachmann, W. Janke, Phys. Rev. E **73**, 041802 (2006)
19. M. Bachmann, W. Janke, Phys. Rev. E **73**, 020901(R) (2006)
20. K. Binder, J. Baschnagel, M. Müller, W. Paul, F. Rampf, Macromol. Symp. **237**, 128 (2006)
21. J. Luettmer-Strathmann, F. Rampf, W. Paul, K. Binder, J. Chem. Phys. **128**, 064903 (2008)
22. S. Karalus, W. Janke, M. Bachmann, Phys. Rev. E **84**, 031803 (2011)
23. M. Bachmann, H. Arkın, W. Janke, Phys. Rev. E **71**, 031906 (2005)
24. F.H. Stillinger, T. Head-Gordon, C. L. Hirshfeld, Phys. Rev. E **48**, 1469 (1993)
25. F.H. Stillinger, T. Head-Gordon, Phys. Rev. E **52**, 2872 (1995)
26. A. Irbäck, C. Peterson, F. Potthast, O. Sommelius, J. Chem. Phys. **107**, 273 (1997)
27. A. Irbäck, C. Peterson, F. Potthast, Phys. Rev. E **55**, 860 (1997)
28. W.A. Steele, Surf. Sci. **36**, 317 (1973)
29. R. Hentschke, Macromol. Theory Simul. **6**, 287 (1997)
30. B.A. Berg, T. Neuhaus, Phys. Lett. B **267**, 249 (1991)
31. B.A. Berg, T. Neuhaus, Phys. Rev. Lett. **68**, 9 (1992)
32. B. A. Berg, T. Çelik, Phys. Rev. Lett. **69**, 2292 (1992)
33. W. Janke, Int. J. Mod. Phys. C **3**, 1137 (1992)
34. B.A. Berg, Fields Inst. Commun. **26**, 1 (2000)
35. W. Janke, Physica A **254**, 164 (1998)
36. B. Efron, *The Jackknife, the Bootstrap and Other Resampling Plans* (Society for Industrial and Applied Mathematics [SIAM], Philadelphia, 1982)
37. W. Janke, *Monte Carlo methods in classical statistical physics, Computational Many-Particle Physics*, Wilhelm & Else Heraeus Summerschool, Greifswald, edited by H. Fehske, R. Schneider, A. Weiße, Lect. Notes Phys. **739** (Springer, Berlin, 2008), p. 79